Oncogene (2021) 40:4384–4397
https://doi.org/10.1038/s41388-021-01871-w

ARTICLE

PELP1/SRC-3-dependent regulation of metabolic PFKFB kinases drives therapy resistant ER$^+$ breast cancer

Thu H. Truong[1] · Elizabeth A. Benner[1] · Kyla M. Hagen[1] · Nuri A. Temiz[1,2] · Carlos Perez Kerkvliet[1] · Ying Wang[1] · Emilio Cortes-Sanchez[3,4] · Chieh-Hsiang Yang[3,4] · Marygrace C. Trousdell[5] · Thomas Pengo[6] · Katrin P. Guillen[3,4] · Bryan E. Welm[3,4,7] · Camila O. Dos Santos[5] · Sucheta Telang[8] · Carol A. Lange[1,9,10] · Julie H. Ostrander[1,9]

Received: 2 December 2020 / Revised: 13 May 2021 / Accepted: 26 May 2021 / Published online: 8 June 2021

Abstract

Recurrence of metastatic breast cancer stemming from acquired endocrine and chemotherapy resistance remains a health burden for women with luminal (ER$^+$) breast cancer. Disseminated ER$^+$ tumor cells can remain viable but quiescent for years to decades. Contributing factors to metastatic spread include the maintenance and expansion of breast cancer stem cells (CSCs). Breast CSCs frequently exist as a minority population in therapy resistant tumors. In this study, we show that cytoplasmic complexes composed of steroid receptor (SR) co-activators, PELP1 and SRC-3, modulate breast CSC expansion through upregulation of the HIF-activated metabolic target genes *PFKFB3* and *PFKFB4*. Seahorse metabolic assays demonstrated that cytoplasmic PELP1 influences cellular metabolism by increasing both glycolysis and mitochondrial respiration. PELP1 interacts with PFKFB3 and PFKFB4 proteins, and inhibition of PFKFB3 and PFKFB4 kinase activity blocks PELP1-induced tumorspheres and protein–protein interactions with SRC-3. PFKFB4 knockdown inhibited in vivo emergence of circulating tumor cell (CTC) populations in mammary intraductal (MIND) models. Application of PFKFB inhibitors in combination with ER targeted therapies blocked tumorsphere formation in multiple models of advanced breast cancer including tamoxifen (TamR) and paclitaxel (TaxR) resistant models, murine tumor cells, and ER$^+$ patient-derived organoids (PDxO). Together, our data suggest that PELP1, SRC-3, and PFKFBs cooperate to drive ER$^+$ tumor cell populations that include CSCs and CTCs. Identifying non-ER pharmacological targets offers a useful approach to blocking metastatic escape from standard of care ER/estrogen (E2)-targeted strategies to overcome endocrine and chemotherapy resistance.

These authors contributed equally: Carol A. Lange, Julie H. Ostrander

Supplementary information The online version contains supplementary material available at https://doi.org/10.1038/s41388-021-01871-w.

✉ Carol A. Lange
lange047@umn.edu

✉ Julie H. Ostrander
hans1354@umn.edu

[1] Masonic Cancer Center, University of Minnesota, Minneapolis, MN, USA

[2] Institute for Health Informatics, University of Minnesota, Minneapolis, MN, USA

[3] Department of Oncological Sciences, University of Utah, Salt Lake City, UT, USA

[4] Huntsman Cancer Institute, University of Utah, Salt Lake City, UT, USA

[5] Cold Spring Harbor Laboratory, Cold Spring Harbor, NY, USA

[6] University of Minnesota Informatics Institute, University of Minnesota, Minneapolis, MN, USA

[7] Department of Surgery, University of Utah, Salt Lake City, UT, USA

[8] James Graham Brown Cancer Center, Department of Medicine (Division of Medical Oncology and Hematology), University of Louisville, Louisville, KY, USA

[9] Department of Medicine (Division of Hematology, Oncology, and Transplantation), University of Minnesota, Minneapolis, MN, USA

[10] Department of Pharmacology, University of Minnesota, Minneapolis, MN, USA

Introduction

Metastatic recurrence is an incurable but common complication of ER^+ breast cancer. Treatment of metastatic breast cancer typically results in endocrine resistance, and chemotherapy is largely ineffective in advanced disease. Altered signaling pathways drive therapy resistance and offer potential targets for metastatic ER^+ breast cancer. Proline, glutamic acid, leucine-rich protein 1 (PELP1) and steroid receptor (SR) co-activator-3 (SRC-3) have independently been shown to drive endocrine resistance. PELP1 and SRC-3 are both SR co-activators involved in normal development and cancer [1, 2]. Increased PELP1 expression is associated with higher tumor grade, tumor proliferation, and decreased breast cancer-specific survival [3, 4]. PELP1 is primarily restricted to the nuclear compartment in normal breast tissue; however, altered cytoplasmic PELP1 localization is observed in 40–58% of PELP1+ breast tumors, which exhibit a wide range of partial to moderate cytoplasmic PELP1 [5]. Analysis of breast tumor samples revealed that patients with high cytoplasmic PELP1 levels were less likely to respond to tamoxifen (tam) [4]. Similarly, increased SRC-3 expression, which occurs in 31–64% of ER^+ breast cancers, is linked to tam resistance [6, 7] and correlated with higher tumor grade and decreased overall and disease-free survival [8]. Both PELP1 and SRC-3 have essential nuclear functions, but also dynamically shuttle to the cytoplasm where they associate with signaling molecules and act as scaffolds for growth factor or SR pathways. These SR co-activators have emerged as promising targets in ER^+ breast cancer and as potential mediators of therapy resistance [9–11].

The cancer stem cell (CSC) hypothesis postulates that tumors contain a subset population (i.e., CSCs) that share properties of normal stem cells including self-renewal, differentiation, and capacity to repopulate the heterogeneous tumor [12]. CSCs are poorly proliferative and frequently exist as a minority sub-population of cells that drive therapy resistance and metastasis [12]. In contrast to non-CSCs, breast CSCs form colonies in serum-free suspension culture (i.e., tumorspheres), express stem cell markers (e.g., $ALDH^+$ or $CD44^{hi}/CD24^{lo}$), and exhibit enhanced resistance to chemo and endocrine therapies. The ability to survive and self-renew following treatment allows CSCs to evade standard therapies aimed at rapidly dividing cancer cells.

Growing evidence has implicated SR co-activators as mediators of CSC self-renewal. For example, SRC-3 drives CSC formation and tumor outgrowth in breast cancer models. Treatment with SI-2, an SRC-3 inhibitor, decreased SRC-3-induced CSCs in breast cancer cell and xenograft models [13]. We previously reported that cytoplasmic complexes composed of PELP1 and SRC-3 mediate breast CSC expansion [14]. Targeting SRC-3 using shRNA or pharmacological inhibitors (i.e., SI-2) abrogated PELP1/SRC-3 complexes, PELP1-induced tumorspheres, and expression of PELP1 target genes that promote cancer cell survival. These studies imply that inhibiting PELP1 and its binding partners may provide a way to target breast CSCs.

Herein we sought to identify the molecular mechanisms that contribute to PELP1-driven CSC survival and self-renewal in ER^+ breast cancer. Our findings in endocrine and chemotherapy-resistant breast cancer models suggest that PELP1/SRC-3 complexes modulate the CSC compartment through gene programs associated with metabolic adaptation. In contrast to current therapies that fail to adequately target slow-growing breast CSCs, our studies reveal therapy combinations that inhibit cooperating signaling cascades while simultaneously targeting ER. By targeting CSCs directly, this approach promises to significantly improve the lives of patients with recurrent ER^+ breast cancer.

Results

Cytoplasmic PELP1 promotes CSCs and HIF-regulated gene expression

Endogenous cytoplasmic PELP1 is readily observed by IHC staining of human breast tumors [4, 5] and in IF staining of human breast samples taken from high-risk women [15]. There are no known in vitro models of endogenous cytoplasmic PELP1. Notably, 3D cultures of breast cancer cells better recapitulate in vivo tumor characteristics (e.g., increased therapy resistance) when compared to 2D cultures [16, 17]. To determine whether the 3D environment alters endogenous PELP1 localization, we evaluated ER^+ and ER^- breast cancer cell lines (MCF-7, SUM225, CCH1) in 2D adherent and 3D Matrigel cultures, and assessed endogenous PELP1 localization by analysis of immunofluorescence images (Supplementary Fig. 1). In all three cell lines tested, the fraction of cytoplasmic PELP1 was significantly increased in 3D relative to 2D cultures (Fig. 1A), suggesting that 3D culture promotes changes in dynamic shuttling of PELP1 to the cytoplasmic compartment. We and others have modeled endogenous cytoplasmic PELP1 by expressing PELP1 containing a nuclear localization signal (NLS) mutation that slows the rate of nuclear translocation and thereby increases steady-state levels of functional cytoplasmic PELP1 [5, 14, 18]. Using these models, we demonstrated preferential binding of SRC-3 to cytoplasmic PELP1 [14]. We confirmed PELP1 localization in these models by immunofluorescence analyses and cellular fractionation in 3D culture (Supplementary Fig. 2).

Our prior work reported cytoplasmic PELP1/SRC-3 signaling complexes increase breast CSCs, as measured by 3D tumorsphere assays [14]. Breast CSCs represent a minority

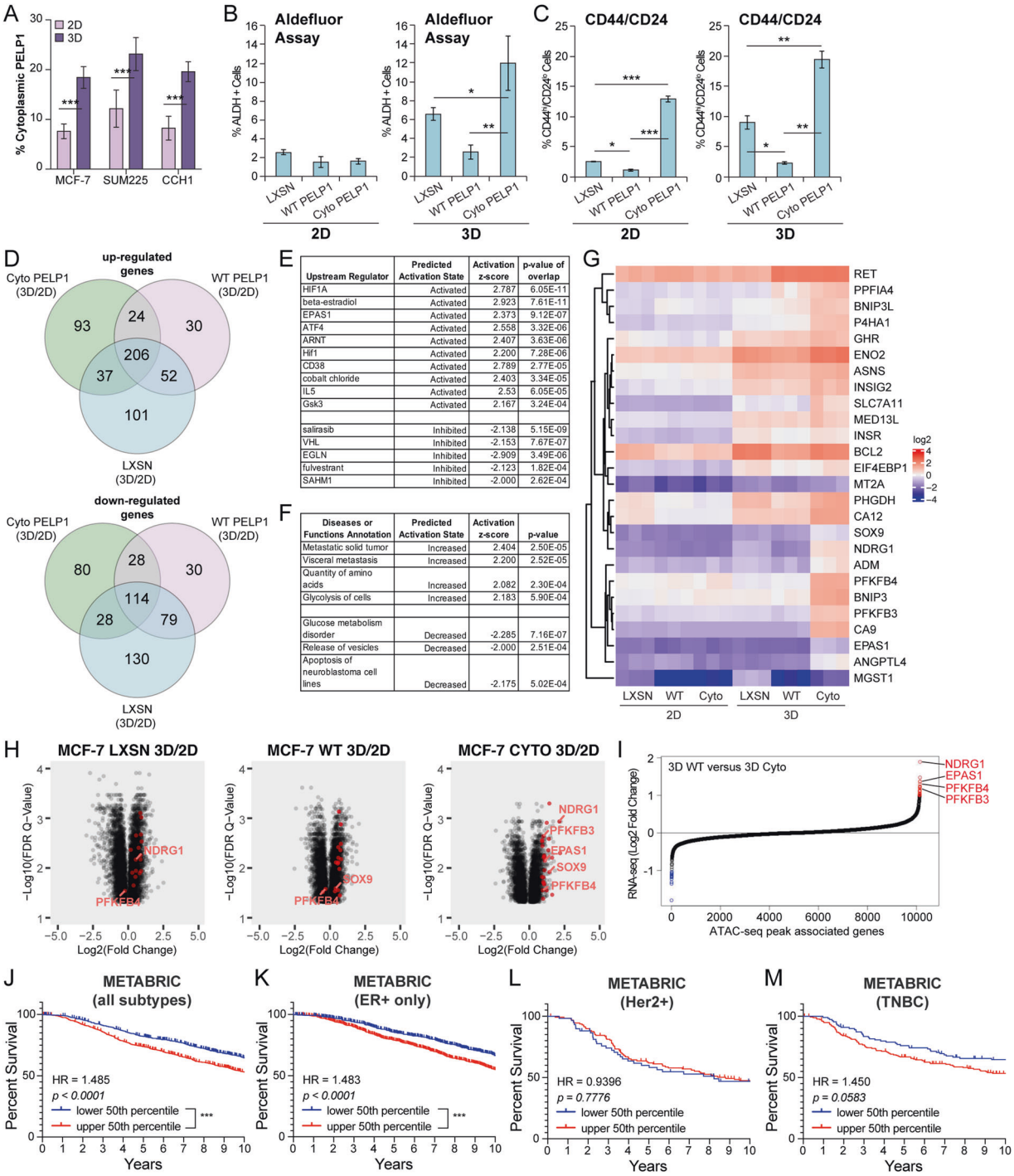

Fig. 1 PELP1-induced gene expression is altered in 3D conditions. **A** Quantification of endogenous cytoplasmic PELP1 in ER$^+$ and ER$^-$ cell lines (MCF-7, SUM225, and CCH1). **B** ALDH$^+$ and **C** CD44^{hi}/CD24^{lo} populations in MCF-7 PELP1 cells. **D** Venn diagrams showing unique genes up or downregulated >2-fold in MCF-7 PELP1 cells (3D vs. 2D). IPA analysis of **E** upstream regulators and **F** diseases or functions. **G** Heat-map showing log2(FPKM) values of cyto PELP1 gene signature. **H** Volcano plots of 3D vs. 2D comparison of MCF-7 PELP1 cells. **I** S-plot showing differentially expressed genes in 3D comparison of MCF-7 WT vs. cyto PELP1 cells from integration of RNA-seq and ATAC-seq analysis. Kaplan–Meier curves for upper and lower 50th percentile of cyto PELP1 gene signature in the METABRIC **J** all subtypes ($n = 1904$), **K** ER$^+$ only ($n = 1222$), **L** Her$^+$ ($n = 188$), and **M** TNBC ($n = 290$) patient cohorts. Graphed data represent the mean ± SD ($n = 3$). *$p < 0.05$, **$p < 0.01$, ***$p < 0.001$.

of the total cell population (1–5%) [19], making it difficult to detect CSC-specific changes in bulk tumor populations. We therefore measured breast CSC frequency by comparing ALDH activity (Fig. 1B and Supplementary Fig. 3) and $CD44^{hi}/CD24^{lo}$ ratios (Fig. 1C and Supplementary Fig. 4) in MCF-7 cells wherein endogenous PELP1 was knocked out [14], followed by stable expression of LXSN (vector control), WT PELP1, or cytoplasmic (cyto; NLS mutant) PELP1; these models were cultured in either 2D (adherent) or 3D (tumorsphere) conditions. Relative to 2D, 3D conditions increased breast CSC markers in MCF-7 cells expressing LXSN, WT PELP1, or cyto PELP1 (Fig. 1B, C). In 2D conditions, cyto PELP1 expressing cells had no significant changes in ALDH activity when compared to LXSN or WT PELP1; however, when the same models were cultured in 3D conditions, ALDH activity was significantly increased in cells expressing cyto PELP1 (12.0% ± 2.9) compared to LXSN (6.6% ± 0.67, $p = 0.023$) and WT PELP1 (2.6% ± 0.76, $p = 0.0015$). In 2D conditions, $CD44^{hi}/CD24^{lo}$ populations were increased in cyto PELP1 expressing cells (13.0% ± 0.49) compared to LXSN (2.6% ± 0.042, $p < 0.0001$) or WT PELP1 (1.2% ± 0.19, $p < 0.0001$), and this trend was enhanced in 3D conditions (cyto PELP1, 19.4% ± 1.4; LXSN, 9.0% ± 1.1, $p = 0.0045$; WT PELP1, 2.3% ± 0.18, $p = 0.0011$). These results indicate that both 3D culture and expression of cyto PELP1 (i.e., relative to WT PELP1) independently increase CSC expansion in MCF-7 cell models.

We next performed RNA-seq on MCF-7 PELP1 models grown as 3D tumorspheres and compared these data to studies conducted in 2D culture [14] to identify candidate genes and pathways differentially regulated in cyto PELP1 expressing cells. Comparison of 3D vs. 2D conditions identified 206 upregulated and 114 downregulated genes similarly regulated by >2-fold in all cell lines (LXSN, WT PELP1, cyto PELP1) (Fig. 1D and Supplementary Fig. 5). Ingenuity Pathway Analysis (IPA) of these 320 genes revealed activation of estrogen, growth factor, cytokine, and NF-κB pathways (Supplementary Table 1). Significantly activated and inhibited "Diseases and Functions" are summarized in Supplementary Table 2. 3D to 2D comparison in cyto PELP1 expressing cells identified 173 differentially expressed genes (93 upregulated, 80 downregulated) compared to LXSN or WT PELP1 (Fig. 1D and Supplementary Fig. 6). These 173 genes were analyzed with IPA to identify cyto PELP1-specific pathways (Fig. 1E), biological functions, or disease states (Fig. 1F), and predicted increased HIF activation, estradiol, ATF4, and glycolytic-mediated pathways. GSEA analysis of 3D cultured cyto PELP1 vs. WT PELP1 also indicated that cyto PELP1 expression affects gene sets associated with cellular metabolism (Supplementary Fig. 7A, B). We then created representative heatmaps to illustrate 3D-specific regulation identified in the IPA upstream regulator analysis associated with HIF and ATF4 pathway activation (>2-fold; Fig. 1G) and generated a cyto PELP1 gene signature from the 26 upregulated genes (Supplementary Table 3). Volcano plots of differentially regulated genes are shown in Fig. 1H; red dots indicate genes in the cyto PELP1 signature. To assess the effect of PELP1 on global chromatin accessibility, we performed ATAC-seq on MCF-7 PELP1 cells (WT and cyto) grown as 3D tumorspheres. Total ATAC-seq peak analysis revealed uniform peak distribution in WT PELP1 and cyto PELP1 3D cultures, suggesting a similar chromatin accessibility landscape (Supplementary Fig. 7C). Additional analyses show that WT PELP1 and cyto PELP1 3D cultures shared the majority of detected ATAC-seq peaks (Supplementary Fig. 7D). Integration of total ATAC-seq peaks with RNA-seq datasets revealed the association of open chromatin sites with differentially expressed genes in cyto PELP1 cells, including *NDRG1, EPAS1, PFKFB3*, and *PFKFB4* (Fig. 1I).

Next, we then used the cyto PELP1 upregulated gene signature (Supplementary Table 3) to query the METABRIC breast cancer database. Higher expression of this gene signature was associated with lower overall survival (OS) in the METABRIC cohort (hazard ratio = 1.485, $p < 0.0001$, Fig. 1J). We tested this on the ER^+ only subtype within the METABRIC cohort and found similar results (hazard ratio = 1.483, $p < 0.0001$, Fig. 1K). No significant differences in OS were found in the Her2+ or TNBC METABRIC cohorts (Fig. 1L, M). A similar query of the TCGA database revealed no significant differences in OS (Supplementary Fig. 8A–D). We also evaluated relapse-free survival in METABRIC (Supplementary Fig. 8E–H) and TCGA (Supplementary Fig. 8I–L) cohorts using the cyto PELP1 upregulated gene signature and observed similar trends with respect to OS. Taken together, these data identify genes involved in cyto PELP1-mediated pathways that promote CSCs, including those associated with HIF-activated and glycolytic pathways.

Cytoplasmic PELP1 drives metabolic plasticity

Given the strong activation of HIF and metabolic pathways detected in the RNA-seq analysis, we used qPCR to test HIF-activated target genes. HIF activates the *PFKFB* family, which are metabolic bi-functional kinase/phosphatases [20]. We found that mRNA levels of *EPAS1* (i.e., HIF2α), *PFKFB3*, and *PFKFB4* were upregulated in cells expressing cyto PELP1 relative to LXSN or WT PELP1 in 3D, but not 2D, conditions (Fig. 2A). Additional validation of HIF-activated metabolic and stem cell genes include *NDRG1* and *SOX9* (Fig. 2A). Given the central role of HIF pathways in metabolism [21], we investigated the effect of PELP1 on metabolic pathways using the Seahorse Cell

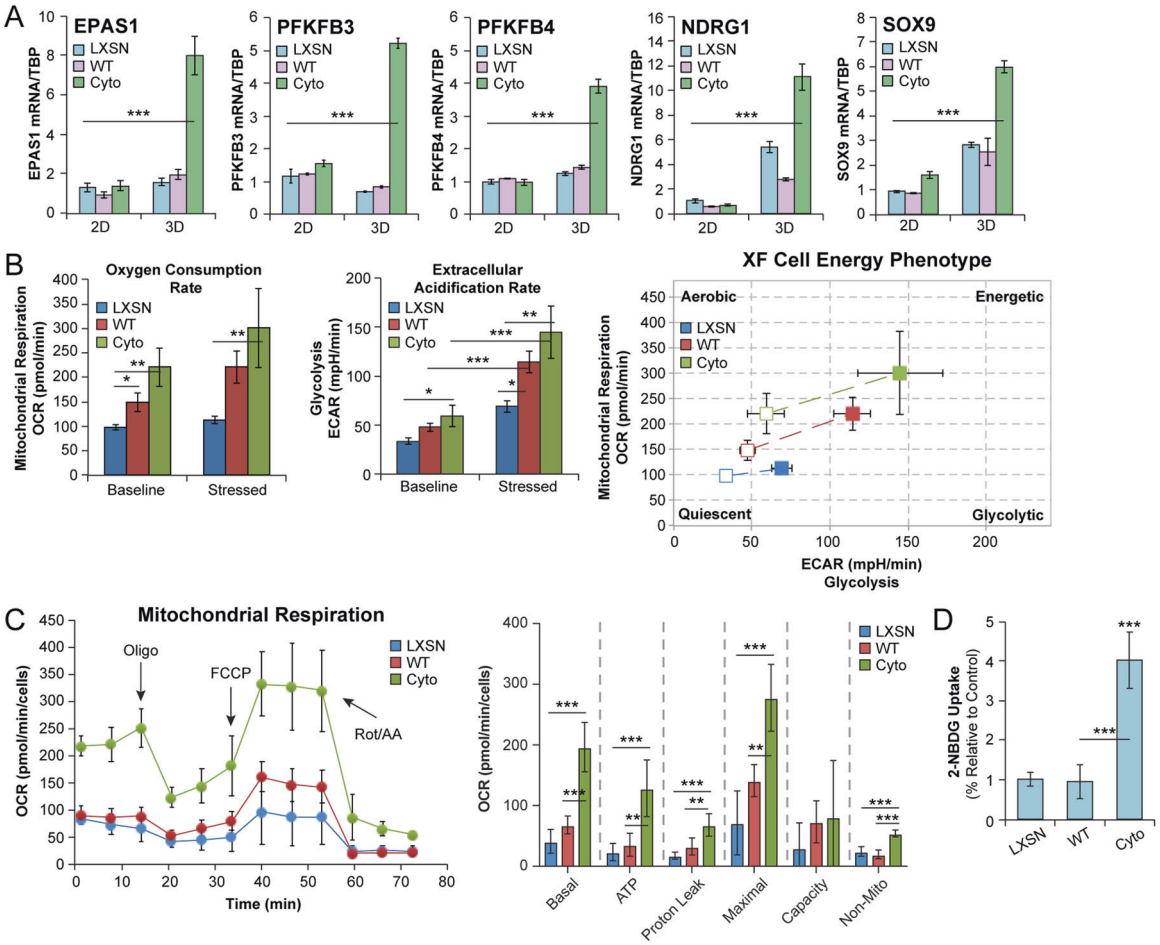

Fig. 2 PELP1 cytoplasmic signaling upregulates HIF-activated metabolic pathways. A mRNA levels of *EPAS1, PFKFB3, PFKFB4, NDRG1*, and *SOX9* in MCF-7 PELP1 cells. **B** OCR and ECAR measured in MCF-7 PELP1 cells by Seahorse Cell Energy Phenotype test. **C** OCR measured in MCF-7 PELP1 cells by Seahorse Mito Stress test. **D** Glucose uptake in cells treated with 2-NBDG. Graphed data represent the mean ± SD ($n = 3$). *$p < 0.05$, **$p < 0.01$, ***$p < 0.001$.

Energy Phenotype test to measure oxygen consumption rate (OCR) and extracellular acidification rate (ECAR). At baseline, MCF-7 cells expressing cyto PELP1 exhibited a significant increase in OCR levels compared to LXSN and WT PELP1. Under stressed conditions (i.e., after FCCP and oligomycin), OCR was increased in cyto PELP1 expressing cells compared to LXSN ($p = 0.0096$). ECAR was significantly different in cyto PELP1 expressing cells compared to LXSN at baseline, but WT and cyto PELP1 displayed an increase in ECAR compared to LXSN controls ($p = 0.046$ and 0.0045) under stressed conditions (Fig. 2B). To systematically test effects on key parameters of mitochondrial function, we performed the Seahorse Mito Stress test. Cyto PELP1 expression significantly increased basal respiration, compared to LXSN and WT PELP1 ($p < 0.0001$ and 0.0001). Furthermore, cyto PELP1 increased ATP-linked respiration, proton leak, maximal respiration, and non-mitochondrial respiration (Fig. 2C). Cyto PELP1 expressing cells had a four-fold increase in glucose uptake compared to WT PELP1 and LXSN, as measured by 2-NBDG (Fig. 2D and Supplementary Fig. 9). Collectively, these results indicate cyto PELP1 drives HIF-activated metabolic programs (i.e., *PFKFB3*, *PFKFB4*) in 3D culture, and affects mitochondrial respiration and glycolysis, indicative of metabolic plasticity.

Inhibition of PFKFBs disrupts PELP1/SRC-3 complexes and tumorsphere formation

We hypothesized that HIF-activated targets PFKFB3 and PFKFB4 are required components of PELP1/SRC-3 complexes. Co-immunoprecipitation of PFKFB3 or PFKFB4 demonstrated increased association with PELP1 in cells expressing cyto PELP1 relative to LXSN or WT PELP1 (Fig. 3A, B). Treatment with PFK158 and 5MPN, inhibitors of PFKFB3 and PFKFB4 respectively, reduced the PELP1/SRC-3 interaction (Fig. 3C, D). Additionally, proximity ligand assays (PLA) showed that the PELP1/SRC-3

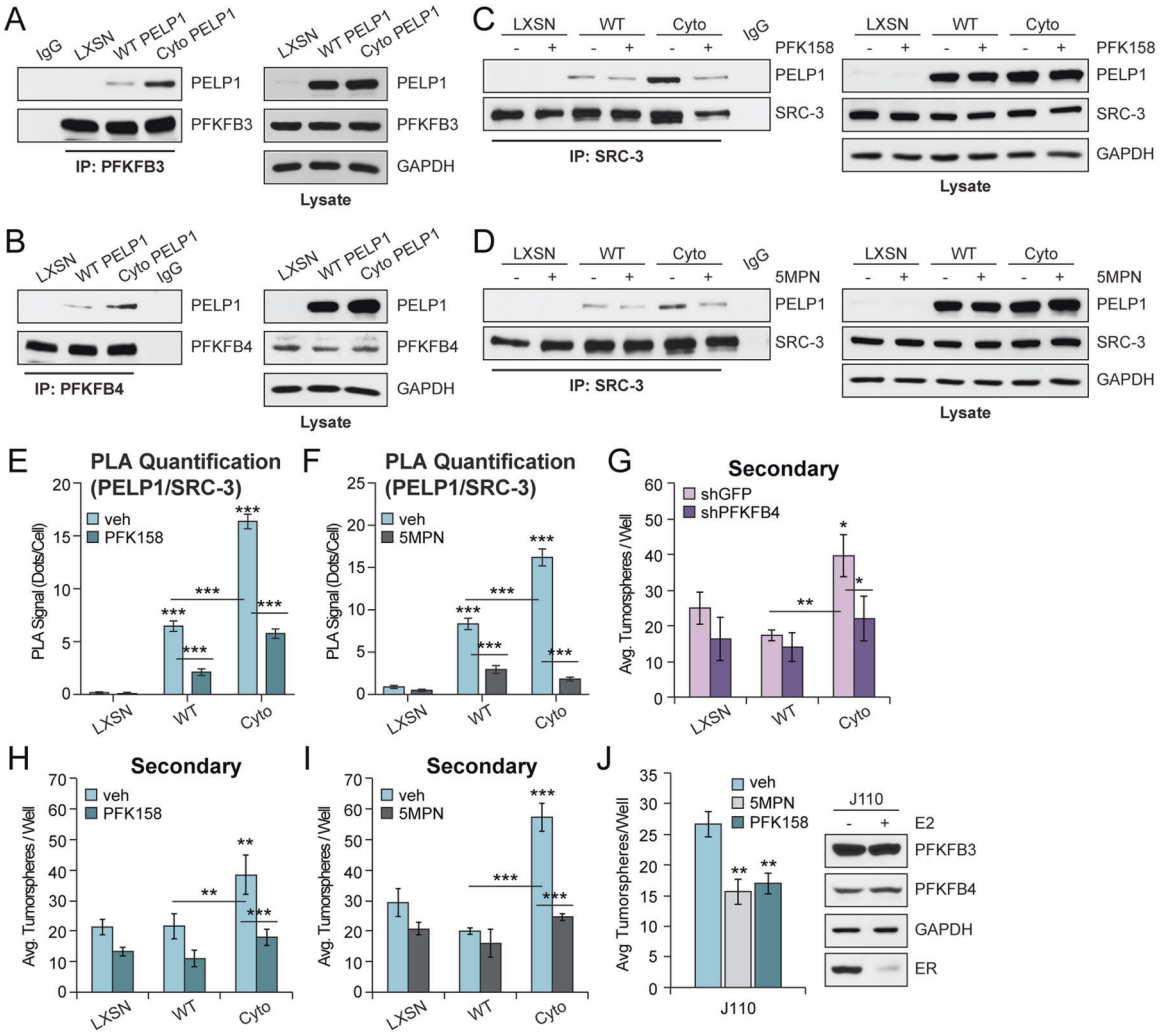

Fig. 3 PFKFB inhibition blocks PELP1/SRC-3 signaling. Co-immunoprecipitation of **A** PELP1 and PFKFB3 or **B** PFKFB4 in MCF-7 PELP1 cells. Co-immunoprecipitation of PELP1 and SRC-3 in MCF-7 PELP1 cells treated with vehicle (DMSO), **C** PFK158 (100 nM), or **D** 5MPN (5 μM). Cell lysate controls (right). Proximity ligand assay (PLA) in MCF-7 PELP1 cells treated with vehicle, **E** PFK158, or **F** 5MPN. **G** Secondary tumorspheres in MCF-7 PELP1 shGFP control and shPFKFB4 knockdown cells. Secondary tumorspheres in MCF-7 PELP1 cells treated with vehicle, **H** PFK158 or **I** 5MPN. **J** Secondary tumorspheres in J110 cells treated with vehicle, PFK158, or 5MPN. Western blot shows PFKFB3 and PFKFB4 levels. Graphed data represent the mean ± SD ($n = 3$). PLA data represent the mean ± SEM. $^{*}p < 0.05$, $^{**}p < 0.01$, $^{***}p < 0.001$.

interaction is reduced upon PFK158 or 5MPN (Fig. 3E, F and Supplementary Fig. 10A, B) treatment. These inhibitors also blocked PELP1/PFKFB3 and PELP1/PFKFB4 (Supplementary Fig. 11A, B) interactions in cyto PELP1 expressing cells; similar results were observed with another PFKFB3 inhibitor (PFK15; Supplementary Fig. 11C, D). Next, we tested the effect of PFKFB inhibition on cyto PELP1-induced tumorspheres, an in vitro assay to assess breast CSC activity [14]. PFKFB4 knockdown (Supplementary Fig. 12) decreased tumorsphere formation in cyto PELP1 expressing cells by ~50%, but not in LXSN or WT PELP1 (Fig. 3G, $p = 0.0103$). Attempts to stably knockdown PFKFB3 were not successful, suggesting that PFKFB3 is crucial for cell viability [22]. Inhibitors of PFKFB3 and PFKFB4 reduced cyto PELP1-induced tumorspheres, but had no effect on cells expressing either LXSN or WT PELP1 (Fig. 3H, I and Supplementary Fig. 11E). We also generated a doxycycline (dox)-inducible PELP1 model in T47D cells (Supplementary Fig. 13A–C). Similar to MCF-7 PELP1 cells, cyto PELP1 expression increased tumorsphere formation (Supplementary Fig. 13D) compared to vector control (pCW) in T47D inducible models. SI-2, PFK158, or 5MPN treatment inhibited tumorsphere formation by 23, 30, and 33% in dox-induced cyto PELP1 cells (Supplementary Fig. 13E). To evaluate PFKFB inhibitors in an alternative PELP1/SRC-3 model, we used a murine tumor cell line (J110) established from the MMTV-SRC-3 mouse [23]. Similar to MCF-7 PELP1

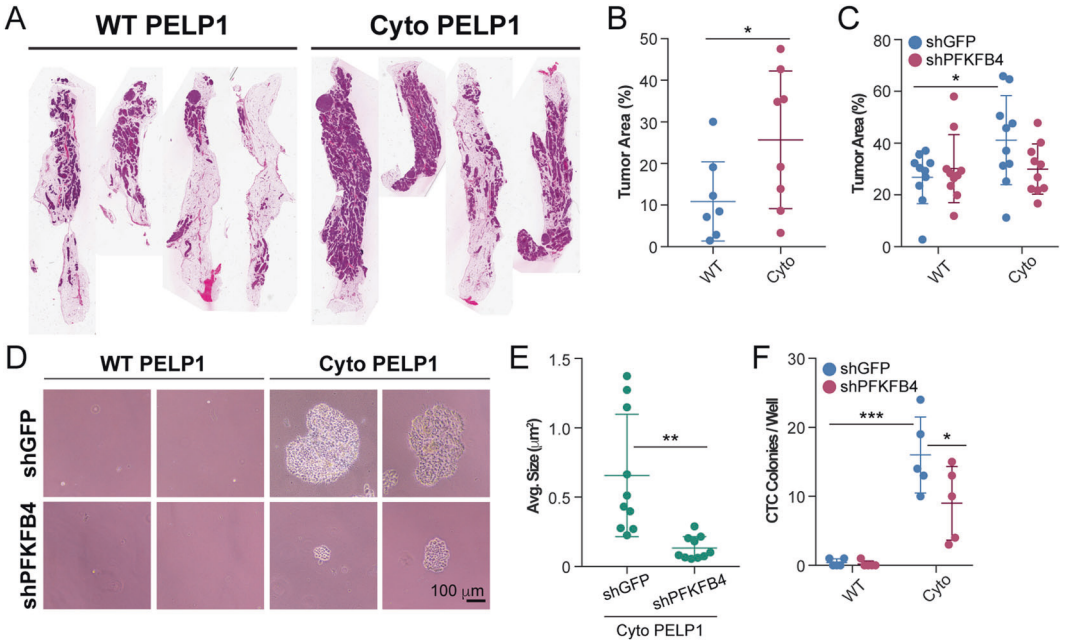

Fig. 4 PFKFB4 knockdown abrogates cyto PELP1 CTCs in MIND xenografts. A Representative H&E stains from MIND glands (WT and cyto PELP1). **B** Tumor area (%) calculated from H&E sections from **A**. **C** Tumor area (%) calculated from H&E sections from WT and cyto PELP1 (shGFP, shPFKFB4) MIND glands. **D** Representative images of CTCs from blood samples collected from mice injected with WT or cyto PELP1 (shGFP, shPFKFB4) cells. **E** Average size of soft agar colonies (CTCs) from **D**. **F** Average number of colonies/well (CTCs). Graphed data represent the mean ± SD ($n = 5$). $*p < 0.05$, $**p < 0.01$, $***p < 0.001$.

models, PFK158 or 5MPN inhibited tumorsphere formation by ~40% in J110 cells (Fig. 3J). Western blotting indicated that PFKFB3 and PFKFB4 protein levels remained unchanged in response to E2, while ER levels decreased, presumably due to ligand-induced turnover (Fig. 3J, right). These results indicate that blocking PFKFB3 or PFKFB4 through knockdown or pharmacological inhibition disrupts expansion and self-renewal of PELP1-driven CSC populations.

PFKFB4 reduces in vivo expansion of CTCs in cyto PELP1 MIND xenografts

The mouse mammary intraductal (MIND) model, wherein cells are injected into the mammary ductal structure via the nipple, has been shown to result in metastatic lesions using ER^+ breast cancer cells [24]. To evaluate if PELP1 promotes tumor formation in vivo, we injected MCF-7 WT and cyto PELP1 expressing cells into the inguinal mammary glands of adult female mice (6–8 week old, 4 mice/group) to generate MIND tumors. Both cell lines had 100% engraftment rates (Fig. 4A and Supplementary Fig. 14). Tumor area (%) calculated from H&E images of each mammary gland revealed increased tumor volume in cyto PELP1 (25.7% ± 16.5) compared to WT PELP1 MIND xenografts (10.9% ± 9.5, $p = 0.046$) (Fig. 4B).

Based on our in vitro data showing that inhibition of PFKFB4 (knockdown and 5MPN) decreased tumorspheres, we queried PFKFB3 and PFKFB4 mRNA levels on OS in METABRIC datasets. PFKFB3 analysis did not yield significant results (Supplementary Fig. 15A, B); however high PFKFB4 mRNA expression is associated with decreased OS in all subtypes and ER^+ only patient cohorts (Supplementary Fig. 15C, D). Therefore, we tested whether PFKFB4 knockdown would impact MIND tumor growth or the presence of circulating tumor cells (CTCs); a marker of metastatic potential and associated CSC behavior [25]. Five mice/group were injected with MCF-7 WT or cyto PELP1 expressing cells harboring either shGFP control or shPFKFB4. Eight weeks postinjection, mammary glands were fixed and processed for H&E staining (Supplementary Fig. 16). As in Fig. 4B, the difference in means between WT PELP1 shGFP (26.8% ± 10.2) and cyto PELP1 shGFP (41.2% ± 17.2) tumor area remained significant ($p = 0.036$, Fig. 4C). However, knockdown of PFKFB4 in MCF-7 cells expressing either WT PELP1 or cyto PELP1 failed to significantly affect primary tumor growth. To assess disseminated tumor cells, blood samples were collected during euthanization and seeded into soft agar assays to detect CTCs. Mice injected with WT PELP1 (shGFP or shPFKFB4) expressing cells did not exhibit CTC colony formation. In sharp contrast, blood samples from mice engrafted with cyto PELP1 cells developed large viable colonies, indicating the presence of CTCs. Knockdown of shPFKFB4 in MCF-7 cyto PELP1 expressing cells reduced both colony

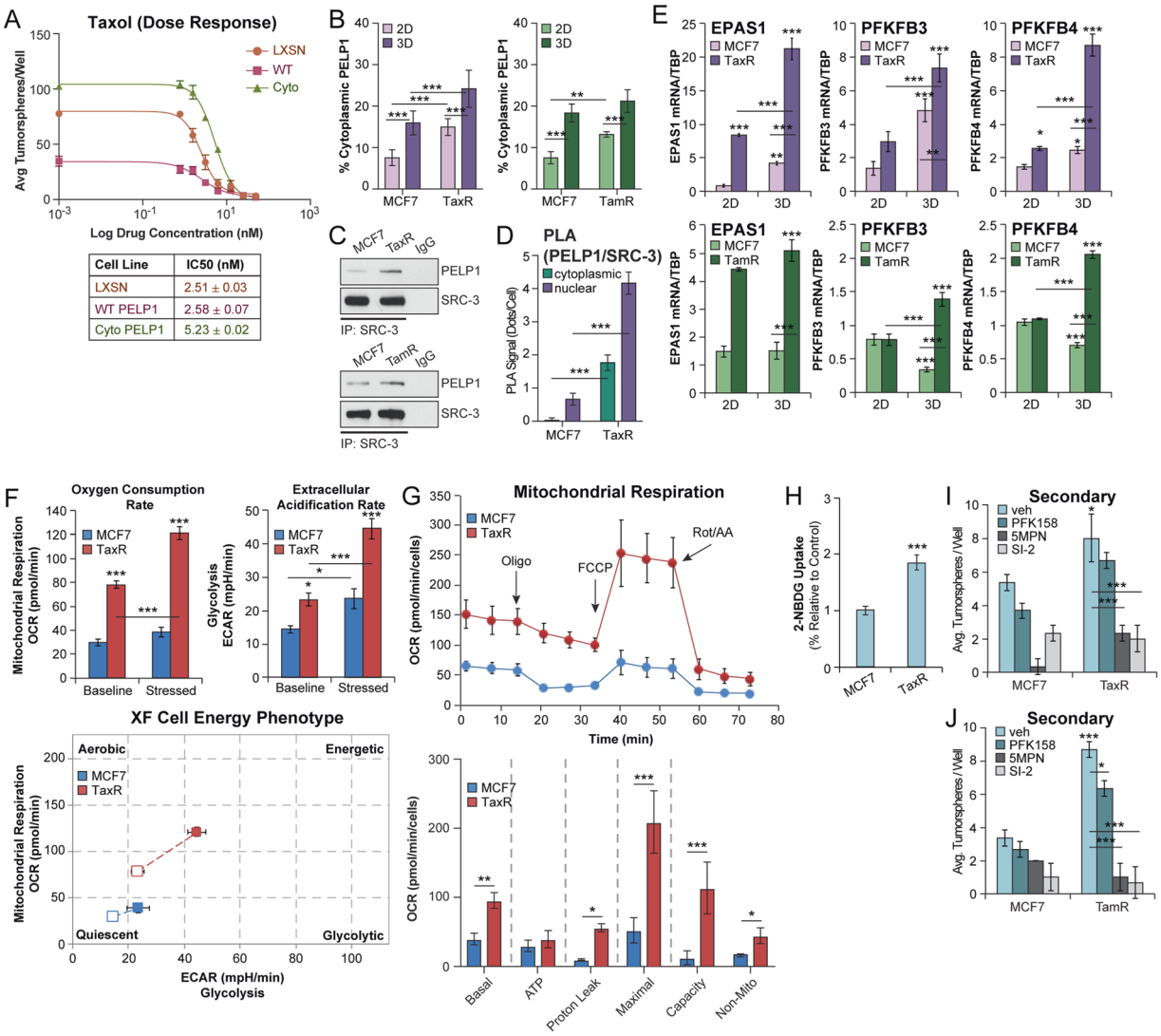

Fig. 5 Therapy resistant models phenocopy cyto PELP1 cancer biology. A Taxol dose response in MCF-7 PELP1 cells (0–50 nM Taxol). **B** Quantification of endogenous cytoplasmic PELP1 in MCF-7 TaxR and TamR cells. **C** Co-immunoprecipitation of PELP1 and SRC-3 in MCF-7 TaxR (top) or TamR (bottom) cells. **D** PELP1/SRC-3 interaction measured by PLA in MCF-7 TaxR cells; quantification of PLA signal (cytoplasmic and nuclear interactions). **E** mRNA levels of *EPAS1, PFKFB3*, and *PFKFB4* in MCF-7 TaxR (top) or TamR (bottom) cells cultured in 2D or 3D conditions. **F** OCR and ECAR measured in MCF-7 TaxR cells by Seahorse Cell Energy Phenotype test. **G** OCR measured in MCF-7 TaxR cells by Seahorse Mito Stress test. **H** Glucose uptake in cells treated with 2-NBDG. Secondary tumorspheres in **I** MCF-7 TaxR and **J** MCF-7 TamR cells treated with vehicle (DMSO), PFK158 (100 nM), 5MPN (5 μM), or SI-2 (100 nM). Graphed data represent the mean ± SD ($n = 3$). *$p < 0.05$, **$p < 0.01$, ***$p < 0.001$.

formation ($p < 0.0492$) and colony size ($p < 0.0016$) (Fig. 4D–F). These data demonstrate a requirement for PFKFB4 in cyto PELP1-driven CTC formation and expansion in vivo.

Targeting PELP1/SRC-3 complexes in therapy resistant breast cancer and PDxO models

Paclitaxel (Taxol) is a chemotherapy used to treat late stage breast cancer. Increased PELP1, HIF1α, and HIF2α expression has also been observed in triple negative breast cancer (TNBC) cells in response to Taxol [26]. To evaluate whether PELP1 expression affects response to Taxol in ER$^+$ breast cancer, we treated MCF-7 PELP1 cells (LXSN, WT PELP1, cyto PELP1) cultured as tumorspheres with Taxol (0–50 nM). We assessed tumorsphere formation and calculated IC50 values for each cell line (Fig. 5A). IC50 (Taxol) for cyto PELP1 expressing cells was ~2-fold higher than LXSN or WT PELP1. These results suggest that cyto PELP1 expression confers enhanced Taxol resistance compared to LXSN or WT PELP1. We also observed increased IC50 (Taxol) for cyto PELP1 expressing cells compared to vector control in T47D dox-inducible PELP1 cells (Supplementary Fig. 13F).

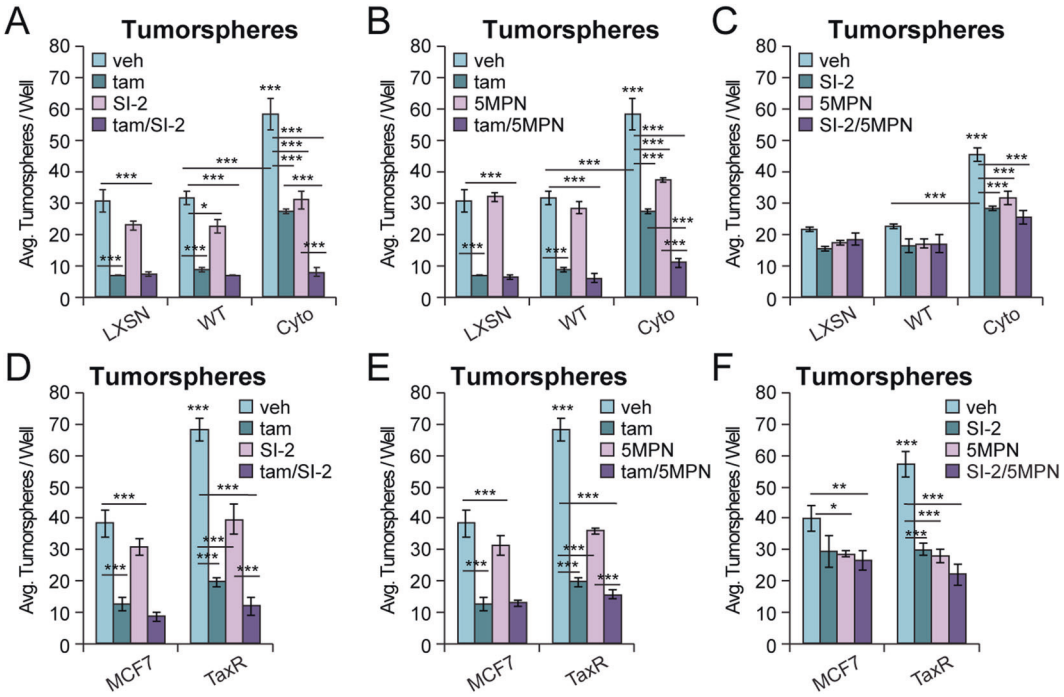

Fig. 6 Endocrine therapies exhibit combinatorial effects with PELP1 complex inhibitors. Tumorsphere assays in MCF-7 PELP1 cells treated with: **A** tam/SI-2, **B** tam/5MPN, or **C** SI-2/5MPN. Tumorsphere assays in MCF-7 TaxR cells treated with: **D** tam/SI-2, **E** tam/5MPN, or **F** SI-2/5MPN. Concentrations: tam (100 nM), 5MPN (5 µM), SI-2 (100 nM). Graphed data represent the mean ± SD ($n = 3$). *$p < 0.05$, **$p < 0.01$, ***$p < 0.001$.

Analysis of 2D adherent and 3D Matrigel cultures demonstrated that endogenous cytoplasmic PELP1 in MCF-7 paclitaxel-resistant (TaxR) and tamoxifen resistant (TamR) cells was significantly increased when compared to controls and also in 3D relative to 2D cultures (Fig. 5B). Interestingly, as we reported in cyto PELP1 models [14], the PELP1/SRC-3 interaction was increased in TaxR (Fig. 5C, top) and TamR cells in co-immunoprecipitation assays (Fig. 5C, bottom). PLA further demonstrated that TaxR cells enhanced endogenous PELP1/SRC-3 complexes in both the cytoplasm and nucleus of intact cells compared to parental controls (Fig. 5D and Supplementary Fig. 17A). PLA also showed that 5MPN reduced PELP1/SRC-3 complexes in TaxR cells (Supplementary Fig. 17B). Additionally, $CD44^{hi}/CD24^{lo}$ ratios were increased in MCF-7 TaxR cells compared to parental controls (Supplementary Fig. 17C, D). Next, we determined if PELP1/SRC-3 signaling mediates therapy resistance in TaxR and TamR cell lines. HIF and cyto PELP1 regulated genes, *EPAS1*, *PFKFB3*, and *PFKFB4* mRNA levels were increased in MCF-7 TaxR (Fig. 5E, top) and TamR cells (Fig. 5E, bottom) relative to parental controls, particularly in 3D conditions. 3D PELP1 target genes, *NDRG1* and *SOX9*, were also upregulated in TaxR and TamR cells relative to parental cells (Supplementary Fig. 18). To determine if similar changes in cellular metabolism occur in MCF-7 TaxR models, we performed Seahorse metabolic assays. The Cell Energy Phenotype test showed TaxR cells exhibit increased OCR and ECAR at baseline and stressed conditions relative to controls (Fig. 5F), indicating increased mitochondrial respiration and glycolysis. To look at individual effects on OCR, we performed the Mito Stress test in MCF-7 TaxR models. Similar to cyto PELP1 expressing cells (Fig. 2C), TaxR cells showed significant increases in basal and maximal respiration compared to controls (Fig. 5G). TaxR cells increased proton leak, spare respiratory capacity, and non-mitochondrial respiration, but not ATP production as observed in MCF-7 cyto PELP1 expressing cells. TaxR cells also displayed ~2-fold increase ($p = 0.0006$) in glucose uptake compared to controls (Fig. 5H). Together, these data reveal that TamR and TaxR models containing endogenous PELP1/SRC-3 complexes phenocopy cyto PELP1 models with regard to elevated HIF-associated target gene expression and metabolic plasticity, and suggest PELP1/SRC-3 signaling may be a key mediator of therapy resistance.

To test the pharmacological effect of PFKFB3, PFKFB4, and SRC-3 inhibition, MCF-7 TaxR and TamR cells were seeded as tumorspheres and treated with PFK158, 5MPN, and SI-2. Both resistant models exhibited increased basal tumorsphere formation when compared to parental controls. 5MPN and SI-2 effectively decreased secondary tumorsphere formation by 71 and 75% in TaxR (Fig. 5I), and 88 and 92% in TamR models (Fig. 5J) compared to vehicle

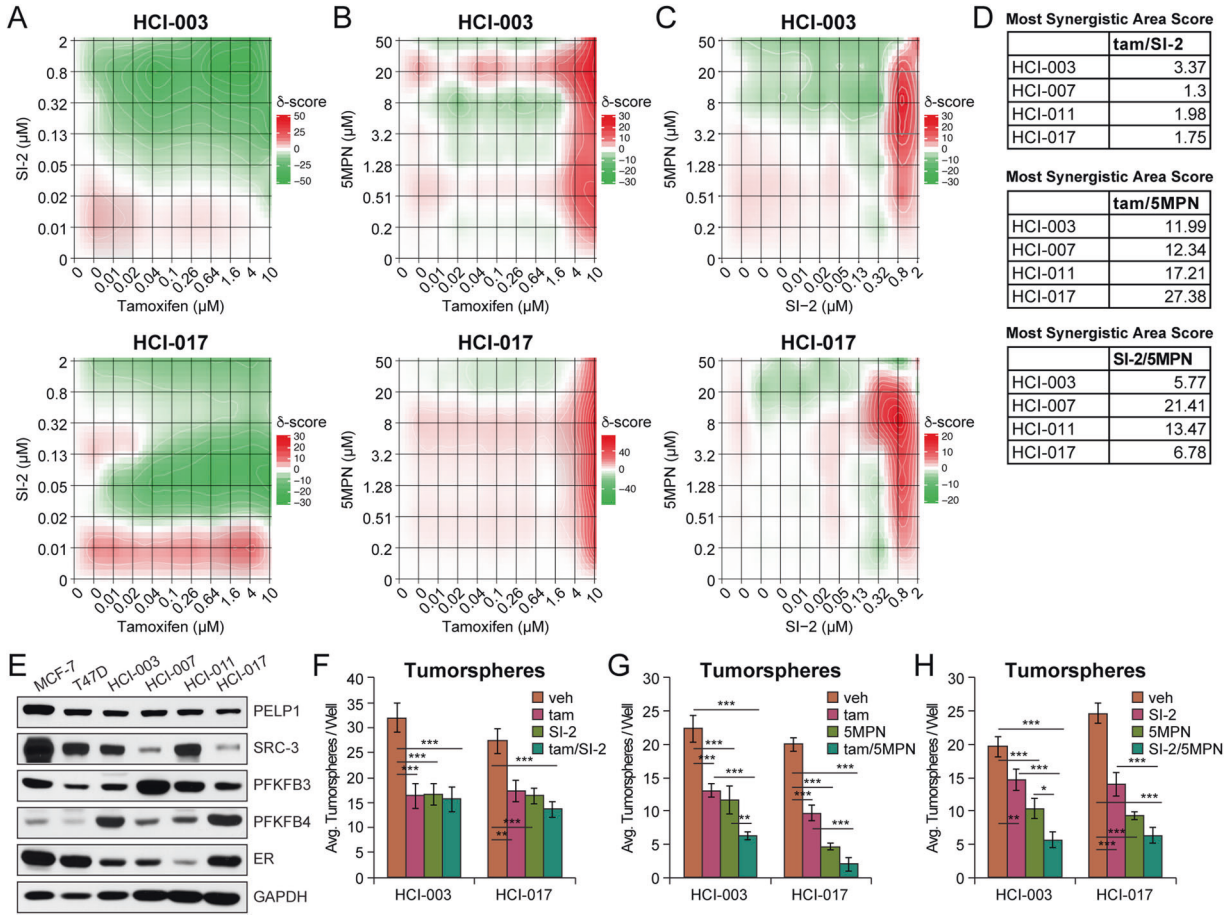

D

Most Synergistic Area Score

	tam/SI-2
HCI-003	3.37
HCI-007	1.3
HCI-011	1.98
HCI-017	1.75

Most Synergistic Area Score

	tam/5MPN
HCI-003	11.99
HCI-007	12.34
HCI-011	17.21
HCI-017	27.38

Most Synergistic Area Score

	SI-2/5MPN
HCI-003	5.77
HCI-007	21.41
HCI-011	13.47
HCI-017	6.78

Fig. 7 Co-treatments in preclinical ER$^+$ PDxO models target CSCs. CellTiter Glo assays in HCI-003 and -017 co-treated with **A** tam/SI-2, **B** tam/5MPN, or **C** SI-2/5MPN. **D** Tables summarizing most synergistic area scores from **A**–**C** and Supplementary Fig. 20A–C. **E** Western blot of PELP1, SRC-3, PFKFB3, PFKFB4, and ER protein in HCI-003, −007, −011, and −017. Tumorsphere assays in HCI-003 and HCI-017 co-treated with **F** tam/SI-2, **G** tam/5MPN, or **H** SI-2/5MPN. Prior to assay, PDxO models were pretreated with the indicated compounds for 3 days and continued treatment during the assay. Concentrations: tam (100 nM), 5MPN (5 μM), SI-2 (100 nM). Graphed data represent the mean ± SD ($n = 3$). *$p < 0.05$, **$p < 0.01$, ***$p < 0.001$.

controls. PFK158 (PFKFB3 inhibitor) modestly decreased TaxR and TamR tumorspheres by 17 and 27%. These findings highlight the overlap of key players involved in PELP1-driven CSC biology and suggest that PFKFB4 and SRC-3 play a more significant role than PFKFB3 within resistant cell models.

We hypothesized that tam in combination with PELP1/SRC-3 complex inhibitors (i.e., SI-2 or 5MPN) would be more effective than either inhibitor alone. Combination treatments were evaluated in several cell lines. In MCF-7 PELP1 models, we tested tam/SI-2, tam/5MPN, and SI-2/5MPN combinations (Fig. 6A–C). Tam/SI-2 and tam/5MPN reduced tumorsphere formation in cyto PELP1 expressing cells by ~85% ($p < 0.0001$) and 80% ($p < 0.0001$) compared to vehicle. Single agent treatment with tam or SI-2 also reduced tumorspheres, but to a lesser degree than combinations. PFK158 co-treatment with tam was not more effective than tam alone and was not further pursued (Supplementary Fig. 19A). Effective combinations were then tested in J110 cells (Supplementary Fig. 19B–D). Tam, SI-2, and 5MPN alone inhibited tumorspheres by 39, 41, and 28%, while co-treatment did not have dramatic effects. The SI-2/5MPN combination was most effective in J110 cells, and decreased tumorsphere formation by 60%, most likely because J110 cells are an SRC-3-derived transgenic mouse mammary tumor cell line [27].

Because PELP1 confers tamoxifen [4, 5] and Taxol (Fig. 5A and Supplementary Fig. 13F) resistance, we also tested the effect of these agents in resistant cell models. Similar to observations in MCF-7 PELP1 models, tam co-treatments were more effective when combined with SI-2 or 5MPN in MCF-7 TaxR models (Fig. 6D, E). The SI-2/5MPN combination was not more effective than individual agents in TaxR models (Fig. 6F), suggesting that SRC-3 and PFKFB4 cooperation occurs in tam-sensitive models. Accordingly, SI-2/5MPN co-treatment in T47D and MCF-7 TamR models reduced tumorsphere formation by 77% ($p < 0.0001$) and 75% ($p < 0.0001$) (Supplementary Fig. 19E, F).

To further explore the therapeutic potential of inhibitor combinations, we utilized preclinical patient-derived organoid models (PDxO) [28]. Synergy screens were used to test combinations identified from Fig. 6 on proliferation using CellTiter Glo assays in PDxO models (HCI-003, -007, -011, and -017). Zero interaction potency scores are shown in contour maps for tam/SI-2, tam/5MPN, and SI-2/5MPN treatments (Fig. 7A–C and Supplementary Fig. 20A–C), and indicate the percent a response is higher (>1) or lower (<1) than the expected response for the dose combination (δ-score). While the δ-score across the range of dose combinations tested were relatively weak, significant peaks of synergism (δ-score > 5) were observed. The most synergistic area scores are summarized in Fig. 7D. The tam/SI-2 δ-scores (~1 to 3) were the lowest and contour maps indicate antagonism. The SI-2/5MPN δ-scores (~5 to 13.5) are lower than the tam/5MPN scores (~12 to 27) suggesting the tam/5MPN combination is more effective at inhibiting PDxO proliferation. Next, we evaluated the ER^+ PDxO models for expression of PELP1, SRC-3, PFKFB3, PFKFB4, and ER mRNA and protein (Supplementary Fig. 20D and Fig. 7E). MCF-7 and T47D cell lines were included as controls. Interestingly, PDxO models have higher levels of PFKFB proteins compared to MCF-7 and T47D cells. Next, we tested inhibitor combinations on CSC activity in PDxO models. PDxOs were grown to maturity, pretreated for 3 days, then dissociated and seeded into tumorspheres in the presence of inhibitors. Individual treatments (tam, SI-2, 5MPN) reduced tumorsphere formation by 36–62% in both PDxO models (Fig. 7F–H). The tam/SI-2 combination was not more effective than individual treatment (Fig. 7F). In contrast, tam/5MPN was more effective than tam or 5MPN alone and reduced tumorspheres by ~71 and ~90% in HCI-003 and HCI-017 (Fig. 7G). SI-2/5MPN co-treatment was more effective than SI-2 or 5MPN alone and reduced tumorsphere formation by ~71% ($p < 0.0001$) and ~74% ($p < 0.0001$) in HCI-003 and HCI-017 (Fig. 7H). These results demonstrate that blocking the PELP1/SRC-3 complex and associated binding partners is an effective approach to targeting CSC populations in multiple models of advanced breast cancer. Taken together, these studies provide promising alternative approaches to target non-ER mediators and overcome emergence of chemotherapy and endocrine resistance.

Discussion

CSCs are proposed to have heightened resistance to cancer therapies due to their relative quiescent state [29], enabling this population to evade standard of care treatments that target proliferating bulk tumor cells. Herein, we sought to define mechanisms of SR co-activator driven CSC survival and expansion in ER^+ breast cancer. We conclude that PELP1/SRC-3 complexes enhance CSC activity and therapy resistance by promoting metabolic plasticity. Inhibiting these complexes and/or associated binding partners in combination with endocrine therapies may be an effective strategy to block CSC survival and self-renewal, and breast cancer progression.

Our findings further implicate PELP1/SRC-3 complexes as mediators of CSC activity. We observed similarities in gene expression, cell metabolism, and sensitivity to inhibitors of PELP1 binding partners in endocrine and chemotherapy-resistant ER^+ cell lines. Although PELP1 expression contributes to cell survival in response to Taxol in TNBC [26], our studies are the first to demonstrate enhanced Taxol tolerance in the context of PELP1 in ER^+ breast cancer. Our results in TaxR models indicate increased endogenous PELP1/SRC-3 cytoplasmic complexes in PLA assays and highlight the impact of targeting PELP1 binding partners involved in PELP1-mediated CSC self-renewal (Fig. 5). Mesenchymal stem cells [30] and ovarian cancer cells [31] achieve Taxol resistance by shifting to G0 and entering quiescence. PELP1 is a substrate of CDKs and modulates G1/S cell cycle progression [32]. PELP1 may confer Taxol resistance in part through cell cycle regulation, albeit further studies are needed to define cytoplasmic PELP1-specific contributions in this context.

Contributing factors to CSC survival include metabolic plasticity, which enables adaptation to diverse tumor environments. For example, inhibition of glycolysis reduces breast and lung CSCs [33]. Glycolytic reprogramming has been documented in breast cancer cells during EMT, resulting in acquisition of CSC-like characteristics and tumorigenicity [34]. In contrast, breast CSCs utilize oxidative phosphorylation (OXPHOS) as their primary metabolic program [35]. Bulk tumor cells depend chiefly on glycolysis, whereas tumors enriched for breast CSCs rely mainly on OXPHOS [36]. RNA-seq analysis indicated cytoplasmic PELP1 imparts increased HIF-activated pathways under normoxic 3D conditions to enrich for CSCs. ChIP assays demonstrated *EPAS1* (i.e., HIF2α) recruitment to HRE regions of the PELP1 promoter in TNBC cells [37]. Thus, PELP1-induced HIF pathways may serve as a feed-forward mechanism to drive metabolic genes programs. PFKFB3 and PFKFB4 are required for glycolytic response to hypoxia via HIF1α activation [20]. We demonstrated that cyto PELP1 expressing cells display increased glycolysis and mitochondrial respiration, and these metabolic phenotypes are recapitulated in therapy resistant breast cancer models. Additional studies are needed to define the bioenergetics driving this plasticity. Both PELP1 and SRC-3 are known to undergo multiple phosphorylation events that occur in the cytoplasm and are required for their nuclear

functions as SR co-activators [38, 39]. Notably, PFKFB4-mediated SRC-3 Ser857 phosphorylation has essential functions in lung and breast cancer metastasis and metabolism [40]. Phosphorylation of SRC-3 Ser857 promotes SRC-3 association with transcription factor *ATF4* to mediate non-oxidative pentose phosphate pathway and purine synthesis. This study [40] did not evaluate SRC-3 in the context of CSCs, although we and others have linked SRC-3 to CSC activity [13, 14]. Our IPA studies also identified ATF4 pathway activation (Fig. 1); upregulation of *ATF4* could explain the correlation between PFKFB4 and PELP1/SRC-3-driven CSCs.

PFKFB inhibitors are emerging as promising treatments in endocrine and chemotherapy-resistant ER^+ breast cancer [41]. PFKFB3 inhibitor PFK158 displays broad anti-tumor and immunomodulatory effects in human and preclinical mouse models [42] and was evaluated in a Phase I clinical trial with no significant adverse effects [43]; however, it did not progress past this stage and is not currently under further clinical development. The prognostic value of PFKFB4 expression was evaluated in 200 tumor samples from stage I to III breast cancer patients. Similar to our METABRIC analysis (Supplementary Fig. 15), elevated PFKFB4 expression was associated with poor disease-free survival and OS in ER^+, $HER2^+$, or TNBC patients [44]. PFKFB4 inhibitors (e.g., 5MPN) have not yet moved to clinical trials. Studies have suggested correlative and mechanistic links between PFKFBs and CSCs. *PFKFB3* was upregulated in a $CD44^{hi}CD24^{lo}$ gene signature correlated to risk of distant metastasis and poor outcome in breast cancer patients [45]. A cleaved product of CD44 (CD44ICD) promoted breast cancer stemness via PFKFB4-mediated glycolysis [46]. We have further implicated PFKFBs as PELP1 binding partners and drivers of CSC activity by demonstrating 5MPN reduces PELP1/SRC-3 complex formation and tumorspheres as a single agent or in combination treatments in multiple ER^+ breast cancer models, including treatment resistant cells (TaxR, TamR), murine tumor cells, and preclinical PDxOs. Our data show that treatment with 5MPN in combination with SI-2 or tam inhibits PDxO proliferation (Fig. 7), but importantly also targets the CSC population. Studies in breast cancer patients indicate that EMT and CSC markers are present in CTC populations, which are markers of increased metastatic potential [47]. Our MIND xenografts demonstrate PFKFB4 knockdown does not have an effect on primary tumor burden but reduces CTC populations (Fig. 4). These data suggest PFKFB4 inhibition is an effective strategy for targeting CSCs and CTCs in ER^+ breast cancer. Future work is aimed at determining the requirement of potential PFKFB-mediated phosphorylation on PELP1 and/or SRC-3 (i.e., in addition to Ser857; [40]) as well as assessing overlap between PFKFB4-modulated CSC and CTC populations by evaluating the impact of 5MPN inhibitor combinations in vivo.

Our work demonstrates that targeting SR co-activators (PELP1, SRC-3) and associated binding partners (PFKFBs) involved in driving CSC survival, self-renewal, and metabolic plasticity may impede breast cancer progression. Identifying the signaling and gene regulatory mechanisms that mediate recurrent ER^+ tumor cell populations (e.g., CSCs, CTCs) will enable specific targeting within heterogeneous breast tumors to overcome endocrine and chemotherapy resistance.

Materials and methods

Cell culture

STR authentication was performed by ATCC (October 2018). Cells were routinely tested for mycoplasma. MCF-7 PELP1 and J110 cells were cultured as described [14]. SUM225 and CCH1 cells were cultured as described [48]. MCF-7 [49] and T47D TamR [50] cells were cultured in 100 nM tamoxifen. MCF-7 TaxR [26] cells were cultured in 2 μM Taxol. For 3D (tumorsphere) conditions, cells were cultured as described [14].

Statistical analysis

Data were tested for normal distribution using Shapiro–Wilks normality test and homogeneity of variances using Bartlett's test. Statistical analyses were performed using one-way or two-way ANOVA in conjunction with Tukey multiple comparison test for means between more than two groups or Student's *t* test for means between two groups, where significance was determined with 95% confidence. For the MIND study with four groups defined by two factors (cyto PELP1 vs. WT PELP1, and shPFKFB4 vs. shGFP), a regression model identified a significant interaction due to shPFKFB4 at an alpha level of 0.1 ($p = 0.084$).

Acknowledgements This work was supported by NIH grants R01 CA236948 (JHO, CAL), R01 CA229697 (CAL), F32 CA210340 (THT), T32 HL007741 (THT), U54 CA224076 (BEW), R01 CA248158-01 (CODS), and R01 AG069727-01 (CODS). ACS Institutional Research Grant #124166-IRG-58-001-52-IRG5 (JHO), University of Minnesota Masonic Cancer Center (CAL, JHO), the Tickle Family Land Grant Endowed Chair in Breast Cancer Research (CAL), National Center for Advancing Translational Sciences of the NIH Award UL1TR000114 (JHO), and Department of Defense W81XWH-14-1-0417 (BEW). We thank Bruce Lindgren for biostatistics support, and the Masonic Cancer Center Biostatistics and Bioinformatics, Analytical Biochemistry, University Imaging Core (UIC), and Flow Cytometry cores. We also thank Zohar Sachs and Michael Franklin for critical reading of this manuscript.

Compliance with ethical standards

Conflict of interest CAL is a Scientific Advisory Board Member for Context Therapeutics, Inc. BEW, EC-S, KPG, and C-HY may receive financial compensation from intellectual property and tangible property licenses managed by the University of Utah. The remaining authors have nothing to disclose.

Publisher's note Springer Nature remains neutral with regard to jurisdictional claims in published maps and institutional affiliations.

References

1. Vadlamudi RK, Wang RA, Mazumdar A, Kim Y, Shin J, Sahin A, et al. Molecular cloning and characterization of PELP1, a novel human coregulator of estrogen receptor alpha. J Biol Chem. 2001;276:38272–9.
2. Xu J, Liao L, Ning G, Yoshida-Komiya H, Deng C, O'Malley BW. The steroid receptor coactivator SRC-3 (p/CIP/RAC3/AIB1/ACTR/TRAM-1) is required for normal growth, puberty, female reproductive function, and mammary gland development. Proc Natl Acad Sci USA. 2000;97:6379–84.
3. Habashy HO, Powe DG, Rakha EA, Ball G, Macmillan RD, Green AR, et al. The prognostic significance of PELP1 expression in invasive breast cancer with emphasis on the ER-positive luminal-like subtype. Breast Cancer Res Treat. 2010;120:603–12.
4. Kumar R, Zhang H, Holm C, Vadlamudi RK, Landberg G, Rayala SK. Extranuclear coactivator signaling confers insensitivity to tamoxifen. Clin Cancer Res. 2009;15:4123–30.
5. Vadlamudi RK, Manavathi B, Balasenthil S, Nair SS, Yang Z, Sahin AA, et al. Functional implications of altered subcellular localization of PELP1 in breast cancer cells. Cancer Res. 2005;65:7724–32.
6. Louie MC, Zou JX, Rabinovich A, Chen HW. ACTR/AIB1 functions as an E2F1 coactivator to promote breast cancer cell proliferation and antiestrogen resistance. Mol Cell Biol. 2004;24:5157–71.
7. Osborne CK, Bardou V, Hopp TA, Chamness GC, Hilsenbeck SG, Fuqua SA, et al. Role of the estrogen receptor coactivator AIB1 (SRC-3) and HER-2/neu in tamoxifen resistance in breast cancer. J Natl Cancer Inst. 2003;95:353–61.
8. Burandt E, Jens G, Holst F, Janicke F, Muller V, Quaas A, et al. Prognostic relevance of AIB1 (NCoA3) amplification and overexpression in breast cancer. Breast Cancer Res Treat. 2013;137:745–53.
9. Song X, Chen J, Zhao M, Zhang C, Yu Y, Lonard DM, et al. Development of potent small-molecule inhibitors to drug the undruggable steroid receptor coactivator-3. Proc Natl Acad Sci USA. 2016;113:4970–5.
10. Ravindranathan P, Lee TK, Yang L, Centenera MM, Butler L, Tilley WD, et al. Peptidomimetic targeting of critical androgen receptor-coregulator interactions in prostate cancer. Nat Commun. 2013;4:1923.
11. Raj GV, Sareddy GR, Ma S, Lee TK, Viswanadhapalli S, Li R. et al. Estrogen receptor coregulator binding modulators (ERXs) effectively target estrogen receptor positive human breast cancers. Elife. 2017;6:e26857.
12. Visvader JE, Lindeman GJ. Cancer stem cells: current status and evolving complexities. Cell Stem Cell. 2012;10:717–28.
13. Rohira AD, Yan F, Wang L, Wang J, Zhou S, Lu A, et al. Targeting SRC coactivators blocks the tumor-initiating capacity of cancer stem-like cells. Cancer Res. 2017;77:4293–304.
14. Truong TH, Hu H, Temiz NA, Hagen KM, Girard BJ, Brady NJ, et al. Cancer stem cell phenotypes in ER($^{+}$) breast cancer models are promoted by PELP1/AIB1 complexes. Mol Cancer Res. 2018;16:707–19.
15. Girard BJ, Regan Anderson TM, Welch SL, Nicely J, Seewaldt VL, Ostrander JH. Cytoplasmic PELP1 and ERRgamma protect human mammary epithelial cells from Tam-induced cell death. PLoS ONE. 2015;10:e0121206.
16. Imamura Y, Mukohara T, Shimono Y, Funakoshi Y, Chayahara N, Toyoda M, et al. Comparison of 2D- and 3D-culture models as drug-testing platforms in breast cancer. Oncol Rep. 2015;33:1837–43.
17. Tasdemir N, Bossart EA, Li Z, Zhu L, Sikora MJ, Levine KM, et al. Comprehensive phenotypic characterization of human invasive lobular carcinoma cell lines in 2D and 3D cultures. Cancer Res. 2018;78:6209.
18. Girard BJ, Knutson TP, Kuker B, McDowell L, Schwertfeger KL, Ostrander JH. Cytoplasmic localization of proline, glutamic acid, leucine-rich protein 1 (PELP1) induces breast epithelial cell migration through up-regulation of inhibitor of kappaB kinase and inflammatory cross-talk with macrophages. J Biol Chem. 2017;292:339–50.
19. Liu Y, Nenutil R, Appleyard MV, Murray K, Boylan M, Thompson AM, et al. Lack of correlation of stem cell markers in breast cancer stem cells. Br J Cancer. 2014;110:2063–71.
20. Chesney J, Clark J, Klarer AC, Imbert-Fernandez Y, Lane AN, Telang S. Fructose-2,6-bisphosphate synthesis by 6-phosphofructo-2-kinase/fructose-2,6-bisphosphatase 4 (PFKFB4) is required for the glycolytic response to hypoxia and tumor growth. Oncotarget. 2014;5:6670–86.
21. Kim JW, Dang CV. Cancer's molecular sweet tooth and the Warburg effect. Cancer Res. 2006;66:8927–30.
22. Shi L, Pan H, Liu Z, Xie J, Han W. Roles of PFKFB3 in cancer. Signal Transduct Target Ther. 2017;2:17044.
23. Torres-Arzayus MI, Font de Mora J, Yuan J, Vazquez F, Bronson R, Rue M, et al. High tumor incidence and activation of the PI3K/AKT pathway in transgenic mice define AIB1 as an oncogene. Cancer Cell. 2004;6:263–74.
24. Sflomos G, Dormoy V, Metsalu T, Jeitziner R, Battista L, Scabia V, et al. A preclinical model for ERalpha-positive breast cancer points to the epithelial microenvironment as determinant of luminal phenotype and hormone response. Cancer Cell. 2016;29:407–22.
25. Kilgour E, Rothwell DG, Brady G, Dive C. Liquid biopsy-based biomarkers of treatment response and resistance. Cancer Cell. 2020;37:485–95.
26. Regan Anderson TM, Ma S, Perez Kerkvliet C, Peng Y, Helle TM, Krutilina RI, et al. Taxol induces Brk-dependent prosurvival phenotypes in TNBC cells through an AhR/GR/HIF-driven signaling axis. Mol Cancer Res. 2018;16:1761–72.
27. Torres-Arzayus MI, Yuan J, DellaGatta JL, Lane H, Kung AL, Brown M. Targeting the AIB1 oncogene through mammalian target of rapamycin inhibition in the mammary gland. Cancer Res. 2006;66:11381–8.
28. Guillen KP, Fujita M, Butterfield AJ, Scherer SD, Bailey MH, Chu Z, et al. A breast cancer patient-derived xenograft and organoid platform for drug discovery and precision oncology. bioRxiv. 2021. https://doi.org/10.1101/2021.02.28.433268.
29. Moore N, Lyle S. Quiescent, slow-cycling stem cell populations in cancer: a review of the evidence and discussion of significance. J Oncol. 2011;2011:396076.
30. Bosco DB, Kenworthy R, Zorio DA, Sang QX. Human mesenchymal stem cells are resistant to Paclitaxel by adopting a non-proliferative fibroblastic state. PLoS ONE. 2015;10:e0128511.

31. Wang X, Pan L, Mao N, Sun L, Qin X, Yin J. Cell-cycle synchronization reverses Taxol resistance of human ovarian cancer cell lines. Cancer Cell Int. 2013;13:77.
32. Nair BC, Nair SS, Chakravarty D, Challa R, Manavathi B, Yew PR, et al. Cyclin-dependent kinase-mediated phosphorylation plays a critical role in the oncogenic functions of PELP1. Cancer Res. 2010;70:7166–75.
33. O'Neill S, Porter RK, McNamee N, Martinez VG, O'Driscoll L. 2-Deoxy-D-Glucose inhibits aggressive triple-negative breast cancer cells by targeting glycolysis and the cancer stem cell phenotype. Sci Rep. 2019;9:3788.
34. Dong C, Yuan T, Wu Y, Wang Y, Fan TW, Miriyala S, et al. Loss of FBP1 by Snail-mediated repression provides metabolic advantages in basal-like breast cancer. Cancer Cell. 2013;23:316–31.
35. Vlashi E, Lagadec C, Vergnes L, Reue K, Frohnen P, Chan M, et al. Metabolic differences in breast cancer stem cells and differentiated progeny. Breast Cancer Res Treat. 2014;146:525–34.
36. Banerjee A, Arvinrad P, Darley M, Laversin SA, Parker R, Rose-Zerilli MJJ, et al. The effects of restricted glycolysis on stem-cell like characteristics of breast cancer cells. Oncotarget. 2018;9:23274–88.
37. Regan Anderson TM, Ma SH, Raj GV, Cidlowski JA, Helle TM, Knutson TP, et al. Breast tumor kinase (Brk/PTK6) is induced by HIF, glucocorticoid receptor, and PELP1-mediated stress signaling in triple-negative breast cancer. Cancer Res. 2016;76:1653–63.
38. Girard BJ, Daniel AR, Lange CA, Ostrander JH. PELP1: a review of PELP1 interactions, signaling, and biology. Mol Cell Endocrinol. 2014;382:642–51.
39. Wu RC, Qin J, Yi P, Wong J, Tsai SY, Tsai MJ, et al. Selective phosphorylations of the SRC-3/AIB1 coactivator integrate genomic reponses to multiple cellular signaling pathways. Mol Cell. 2004;15:937–49.
40. Dasgupta S, Rajapakshe K, Zhu B, Nikolai BC, Yi P, Putluri N, et al. Metabolic enzyme PFKFB4 activates transcriptional coactivator SRC-3 to drive breast cancer. Nature. 2018;556:249–54.
41. Mondal S, Roy D, Sarkar Bhattacharya S, Jin L, Jung D, Zhang S, et al. Therapeutic targeting of PFKFB3 with a novel glycolytic inhibitor PFK158 promotes lipophagy and chemosensitivity in gynecologic cancers. Int J Cancer. 2019;144:178–89.
42. Telang S, Yaddanapudi K, Grewal J, Redman R, Fu S, Pohlmann P, et al. Abstract B90: PFK-158 is a first-in-human inhibitor of PFKFB3 that selectively suppresses glucose metabolism of cancer cells and inhibits the immunosuppressive Th17 cells and MDSCs in advanced cancer patients. Cancer Res. 2016;76:B90.
43. Redman R, Pohlmann P, Kurman M, Tapolsky GH, Chesney J. Abstract CT206: PFK-158, first-in-man and first-in-class inhibitor of PFKFB3/ glycolysis: a phase I, dose escalation, multi-center study in patients with advanced solid malignancies. Cancer Res. 2015;75:CT206.
44. Yao L, Wang L, Cao ZG, Hu X, Shao ZM. High expression of metabolic enzyme PFKFB4 is associated with poor prognosis of operable breast cancer. Cancer Cell Int. 2019;19:165.
45. Marotta LL, Almendro V, Marusyk A, Shipitsin M, Schemme J, Walker SR, et al. The JAK2/STAT3 signaling pathway is required for growth of CD44(+)CD24(−) stem cell-like breast cancer cells in human tumors. J Clin Invest. 2011;121:2723–35.
46. Gao R, Li D, Xun J, Zhou W, Li J, Wang J, et al. CD44ICD promotes breast cancer stemness via PFKFB4-mediated glucose metabolism. Theranostics. 2018;8:6248–62.
47. Giordano A, Gao H, Anfossi S, Cohen E, Mego M, Lee BN, et al. Epithelial-mesenchymal transition and stem cell markers in patients with HER2-positive metastatic breast cancer. Mol Cancer Ther. 2012;11:2526–34.
48. Behbod F, Kittrell FS, LaMarca H, Edwards D, Kerbawy S, Heestand JC, et al. An intraductal human-in-mouse transplantation model mimics the subtypes of ductal carcinoma in situ. Breast Cancer Res. 2009;11:R66.
49. Yang Y, Chan JY, Temiz NA, Yee D. Insulin receptor substrate suppression by the tyrphostin NT157 inhibits responses to insulin-like growth factor-I and insulin in breast cancer cells. Horm Cancer. 2018;9:371–82.
50. Dwyer AR, Truong TH, Kerkvliet CP, Paul KV, Kabos P, Sartorius CA, et al. Insulin receptor substrate-1 (IRS-1) mediates progesterone receptor-driven stemness and endocrine resistance in oestrogen receptor+ breast cancer. Br J Cancer. 2021;124:217–27.